Solid ^{4}He and the diffusion Monte Carlo method: A study of their properties

E. J. Rugeles,[1] Sebastian Ujevic,[2] and S. A. Vitiello[1]

[1]*Instituto de Física Gleb Wataghin, Universidade Estadual de Campinas—UNICAMP, 13083-970 Campinas, SP, Brazil*

[2]*Departamento de Ciências Exatas—EEIMVR, Universidade Federal Fluminense, 27255-125 Volta Redonda, RJ, Brazil*

(Received 6 February 2017; revised manuscript received 8 May 2017; published 11 October 2017)

Properties of helium atoms in the solid phase are investigated using the multiweight diffusion Monte Carlo method. Two different importance function transformations are used in two series of independent calculations. The kinetic energy is estimated for both the solid and liquid phases of ^{4}He. We estimate the melting and freezing densities, among other properties of interest. Our estimates are compared with experimental values. We discuss why walkers biased by two distinctly different guiding functions do not lead to noticeable changes in the reported results. Criticisms concerning the bias introduced into our estimates by population control and system size effects are considered.

DOI: 10.1103/PhysRevE.96.043306

I. INTRODUCTION

The systems formed by helium atoms are among the most studied in condensed matter physics. Nevertheless, even after decades of research, solid ^{4}He continues to produce surprises [1]. Two of the phenomena challenging both experimentalists and theoreticians are ^{4}He mass flux through solid helium [2,3] and giant plasticity [4]. Much more work is needed in order to unravel all the properties of quantum crystals made from ^{4}He atoms.

In the last several decades, a variety of models based on wave functions of the Jastrow-Feenberg [5] form have been proposed to deepen our understanding of solid ^{4}He [6–8]. Its simplest description is given by the Nosanow-Jastrow (NJ) wave function. It is built by a product of factors, one that correlates pairs of particles and another which localizes atoms around lattice sites chosen *a priori*. The explicit inclusion of three-body terms [9] and the introduction of the basis set approach [7] significantly improved the results [10]. In an alternative approach, the ideas introduced by shadow wave functions [11] avoided some difficulties of the previously mentioned trial functions. Instead of one-body terms which destroy fundamental properties of the system, such as symmetry under particle exchange and translational invariance, a set of auxiliary variables integrated within the whole space was used. This successful class of wave functions considers implicit correlations up to the number of particles in the system.

Not long ago the symmetric Nosanow-Jastrow (SNJ) trial wave function was introduced [6] into the literature. This ansatz made it possible to symmetrize the Nosanow one-body term without using a permanent. This avoids the associated burden found in most calculations that use a permanent in the symmetrization of a wave function. It gave impressive results in the variational study of the helium quantum solid-liquid phase transition [12]. Results obtained with the SNJ and NJ trial functions can be quite different. See, for instance, the one-body density matrix produced by these trial functions [6]. The SNJ shows an off-diagonal long-range order whereas the NJ trial function does not have this property.

Development of variational wave functions continues to be a topic of interest in the literature. For instance, Lutsyshyn [13] generalized the SNJ trial function to describe coordination shells in the liquid phase of systems formed from ^{4}He atoms. Very recently [14], a systematic discussion of the lowest-order constrained variational method [15] led to a construction of high quality two-body factors. Hopefully those efforts together with this paper might give hints for the construction of a wave function, where a solid phase emerges as a consequence of a symmetry breaking due to many-body effects, without an *a priori* chosen crystalline structure or a set of auxiliary variables.

Properties of physical interest associated with these wave functions are efficiently computed by the variational Monte Carlo method. This is one of the simplest approaches for dealing with quantum many-body problems. An upper bound of the ground state energy of the system can be determined by the optimization of the variational parameters. In spite of many insights that this method is able to give, two issues need to be considered. The first one is how to increase the accuracy of the variational functions through functional forms that more realistically reflect the actual properties of the system. The second one is the optimization of parameters. However, note that these issues have been alleviated to some degree by the basis set approach [7] and by the development of efficient optimization methods; see, for instance, Ref. [16].

The variational method is important due to the insights it brings to enlarge our comprehension of numerous problems. Moreover, the resulting trial function associated to this method is a very important ingredient of the diffusion Monte Carlo (DMC) method used in this paper. The DMC is an "exact" method at zero temperature. Using configurations drawn from a trial function it projects out the ground state of the system. Additionally, in many cases it is crucial to use a trial function as a guiding function, biasing the random walk into important regions of the configuration space. It is relevant to stress that the algorithm is insensitive to a particular guiding function used in the importance sampling transformation, as long it does not exclude significant regions of the configuration space.

The importance sampling transformation has a zero variance property; i.e., as a guiding function converges to the ground state wave function, the local energy goes to the eigenvalue E_0 of the ground state in the entire configuration space [17–19]. This can only be accomplished by a symmetric wave function if the system obeys the Bose-Einstein statistics. These transformations are particularly simple and useful for the study of systems formed by ^{4}He atoms. This is because, in accordance with Feynman [20], the ground state of a system

 ©2017 American Physical Society

formed from bosons can be described by a real wave function without nodes. Moreover, as the guide function becomes more realistic, the statistical uncertainties of the results decrease and the convergence to the ground state is faster. It is also well known that in certain situations small adjustments in the guide function may produce significant changes in the results; consider, for instance, the consequences of small displacements in the nodal structure of a guide function in simulations of systems formed from fermions [21].

The aim of the present paper is twofold. Since the role of statistics is crucial for systems like those formed from ^{4}He atoms [22], we want to understand how the implementation of the SNJ guiding function will affect DMC results, which are often obtained considering only the simpler NJ. It is also our aim to learn about the accuracy of our implementation of the diffusion Monte Carlo method, with respect to bias in the results due to both the system size and the number of walkers in the simulation.

In this paper, both NJ and SNJ are used as guiding functions in two series of independent calculations. Several physical properties of systems of ^{4}He atoms in the solid phase were computed, and the results were analyzed to show possible changes due to these two quite different guiding functions. We compute the pressure at which the solid-liquid quantum phase transition occurs by evaluating the Gibbs free energy of the system. This thermodynamic analysis will also allow the calculation of the melting and freezing densities. The estimated values of these properties are also compared with those obtained by the more common Maxwell double tangent construction.

Another quantity we estimate is the kinetic energy. Its calculation, performed using the multiweight diffusion Monte Carlo method [23], can be made practically without any additional computational cost when evaluating the ground state energy. This is an attractive quantity to estimate because it is one of the most widely studied properties of ^{4}He in experiments using neutrons [24]. Additionally, this quantity might be technically relevant in the context of Monte Carlo projection methods. Possibly, the total energy calculation might have a bias proportional to the expectation value of the kinetic energy [25].

Population control bias and size effects are two factors that could impact our conclusions and for this reason we have carefully considered them in our paper. For the many-body system in our study the importance sampling transformation seems to be essential and does not affect the results within the statistical uncertainties. Nevertheless it has been noticed [26] that importance sampling transformations performed in DMC calculations may bias the results.

Our paper is organized as follows. In the next section we give the description used to characterize the helium atom system we are considering. In a subsection we give details about the guiding functions used in our calculations. The standard DMC method can be seen as a particular case of the multiweight DMC used to implement the Feynman-Hellmann theorem [27] through which we compute the kinetic energies. Therefore we decided to give a brief account of the diffusion Monte Carlo with the multiweight extension. Then we discuss how the simulations and the bias analyses were performed. In Sec. III, we present equations of state for both the liquid and solid phase used to estimate the melting and freezing transitions. The total, kinetic, and potential energy estimates are also given. In the last section, we discuss the relative merits of the two guiding functions we have analyzed.

II. METHOD

Properties of systems formed from ^{4}He atoms can be estimated by considering the Hamiltonian

$$H = -\frac{\hbar^2}{2m}\sum_{i=1}^{N}\nabla_i^2 + \sum_{i<j}V(r_{ij}), \tag{1}$$

where N is the number of atoms and $V(r_{ij})$ is the interaction potential that depends only on interatomic distance $r_{ij} = |\mathbf{r}_i - \mathbf{r}_j|$. We have considered the analytic representation of the potential using the damped Hartree-Fock-dispersion form dubbed HFD-B3-FCI1 proposed by Aziz and coworkers [28]:

$$V(x = r/r_m) = \epsilon\left[A\exp[-(\alpha x+\beta x^2)] - B(x)\sum_{j=0}^{2}\frac{C_{2j+6}}{x^{2j+6}}\right], \tag{2}$$

where r_m is the minimum of the potential. The values of the parameters ϵ, A, α, β, and C_i can be found in Ref. [28]. The function $B(x) = \exp[-(\frac{D}{2}-1)^2]$ depends on parameter D. It dumps the dispersion coefficients C_i if $x \leqslant D$, otherwise it is equal to 1.

Diffusion Monte Carlo is the standard method to determine the ground state energy of this system. This is accomplished by the simulation in imaginary time of the corresponding classical diffusion process with a source $V(r)$. In general, this process needs to be guided by a trial wave function $\psi_G(\mathbf{R})$ able to give a meaningful description of the ground state. For efficiency, branching of configurations is introduced to avoid the burden of keeping configurations that do not give practically any contribution to the results. After a long enough "time," configurations are distributed according to $\psi_G(\mathbf{R})\psi_0(\mathbf{R})$, where $\psi_0(\mathbf{R})$ is the ground state eigenfunction of the Hamiltonian, Eq. (1).

A. Guiding functions

In the solid phase, we have considered runs using the NJ guiding function and another independent series of runs employing SNJ. For our purposes, a guiding function of the Jastrow form $\psi_J(\mathbf{R})$ in the liquid phase is enough.

1. The Nosanow-Jastrow function

The Nosanow-Jastrow wave function is the simplest form that is able to give meaningful results for helium atoms in the solid phase. It is formed by a product of factors that correlate pairs of atoms multiplied by a product of one-body terms that localize the atoms in an *a priori* given crystalline structure, of sites $\{\mathbf{l}_i\}$:

$$\Psi_{NJ} = \psi_J(\mathbf{R})\Phi(\mathbf{R}), \tag{3}$$

$$\psi_J(\mathbf{R}) = \prod_{i<j}^{N} \exp\left[-\frac{b}{2}\left(\frac{1}{r_{ij}}\right)^5\right], \tag{4}$$

$$\Phi(\mathbf{R}) = \prod_{i=1}^{N} \exp\left[-\frac{c}{2}|\mathbf{r}_i - \mathbf{l}_i|^2\right]. \tag{5}$$

In the above expressions $\mathbf{R} = \{\mathbf{r}_1, \ldots, \mathbf{r}_N\}$, b, and c are parameters. Note that this guiding function is neither symmetric under particle exchange nor translational invariant.

2. *The symmetric Nosanow-Jastrow function*

This is a symmetric guiding function that, nevertheless, is not translational invariant:

$$\Psi_{\mathrm{SNJ}}(\mathbf{R}) = \psi_J(\mathbf{R}) \prod_j \sum_i \exp\left[-\frac{c}{2}|\mathbf{r}_i - \mathbf{l}_j|^2\right]. \tag{6}$$

In this function any atom can be found around any lattice site. The product of the sums gives all the terms that consider permutations of particles and sites plus terms where a single particle can be around different lattice sites. The last terms will almost surely be small compared with those that take into account legitimate permutations. In general, this is true because if a particle is near a given lattice site it cannot be simultaneously near another one. It is also important to note that we will never find an empty site. In this function, the occupancy of the sites is constitutively imposed by the product of Gaussian factors. If this condition is not met, the system goes to a liquid or glassy phase [6].

B. The diffusion Monte Carlo method with multiweights

In a standard DMC calculation, the estimation of quantities that do not commute with the Hamiltonian is less than optimal. For instance, the kinetic energy can be obtained by extrapolation [29]. However, this introduces a bias due to the need for a variational estimation of this quantity performed with ψ_{G}. In this case, an alternative is to implement the Feynman-Hellmann theorem using the multiweight DMC method. It allows us to obtain the kinetic energy from the estimated values of the potential and total energies, without the above mentioned bias. The multiweight DMC method is easily implemented and is used in this paper.

The Feynman-Hellmann theorem allows the potential energy E_P to be computed by the derivative with respect to a parameter λ of the expected value of the Hamiltonian where the substitution $V \to \lambda V$ was applied:

$$E_P \equiv \frac{d}{d\lambda}\langle H(\lambda)\rangle\Big|_{\lambda=1} = \frac{d}{d\lambda}E^{\lambda}\Big|_{\lambda=1}, \tag{7}$$

with the brackets denoting averages over configurations and E^{λ} the total energy. Finally the kinetic energy E_K is computed through

$$E_K = E^{(\lambda=1)} - E_P. \tag{8}$$

In the implementation of the Feynman-Hellmann theorem through the multiweight extension of the DMC method, three different weights are associated to a given configuration or walker. The weights are computed for the $\lambda = \{1-\delta, 1, 1+\delta\}$ values, where δ is a parameter small enough for the numerical derivatives about $\lambda = 1$ to be computed with the necessary accuracy. Our results are insensitive to a particular value chosen for δ. The weights are independently treated and the total energies of the systems are computed for each Hamiltonian $H(\lambda)$. Of course, a total energy corresponding to a particular value of λ should agree within statistical uncertainties, with the result obtained by the standard DMC simulation using the Hamiltonian $H(\lambda)$.

A single set of walkers is generated for all Hamiltonians $H(\lambda)$. In this way, the total energies E^{λ} will have correlated statistical fluctuations. Therefore, the numerical derivatives required by the Feynman-Hellmann theorem can be performed with the needed accuracy.

The drift of a given configuration $\mathbf{R}$ can be kept unique without any difficulty for all the values of λ. A new configuration $\mathbf{R}'$ is sampled from $\mathbf{R}$ according to the standard procedure:

$$G_d(\mathbf{R},\mathbf{R}') = \left(\frac{1}{4\pi D\Delta\tau}\right)^{-3N/2} \times \exp\left[-\frac{1}{4D\Delta\tau}|\mathbf{R}' - \mathbf{R} - D\Delta\tau\mathbf{F}(\mathbf{R})|^2\right], \tag{9}$$

where $D = \hbar^2/2m$ is the diffusion constant, $\Delta\tau$ is the "time" step, and $\mathbf{F} = 2\nabla \ln \Psi_G$.

The three weights ω'^{λ} associated to a given walker are updated in the usual way $\omega^{\lambda} = \omega'^{\lambda} G_b^{\lambda}(\mathbf{R},\mathbf{R}')$ using the factors

$$G_b^{\lambda}(\mathbf{R},\mathbf{R}') = \exp\left[-\frac{\Delta_{\mathrm{eff}}\tau}{2}\left[E_L^{\lambda}(\mathbf{R}) + E_L^{\lambda}(\mathbf{R}') - 2E_{\mathrm{trial}}^{\lambda}\right]\right]. \tag{10}$$

In this expression, $E_L^{\lambda} = H(\lambda)\Psi_T/\Psi_T$ are local energies and $E_{\mathrm{trial}}^{\lambda}$ are trial energies. We compute the weights, considering the actual time step in which the atoms are diffusing. The effective time step we use is given [19] by

$$\Delta\tau_{\mathrm{eff}} = \frac{\langle(\Delta R)^2_{\mathrm{acc}}\rangle}{\langle(\Delta R)^2\rangle}\Delta\tau, \tag{11}$$

where $\langle(\Delta R)^2_{\mathrm{acc}}\rangle$ is the mean-squared distance effectively accepted in the diffusion process of the atoms and $\langle(\Delta R)^2\rangle$ is the proposed value of this quantity.

The energies E_{ℓ}^{λ} in the ℓth generation are calculated using the weights ω_i^{λ} and the local energies for all walkers $\mathbf{R}_i$:

$$\frac{\langle\psi_G|H(\lambda)|\psi_0\rangle}{\langle\psi_G|\psi_0\rangle} \approx E_{\ell}^{\lambda} = \frac{\sum_i \omega_i^{\lambda} E^{\lambda}(\mathbf{R}_i)}{\sum_i \omega_i^{\lambda}}. \tag{12}$$

Once the total energies are estimated, the kinetic and potential energies are computed through

$$E_P = \frac{E_{\ell}^{1+\delta} - E_{\ell}^{1-\delta}}{2\delta}, \quad E_K = E_L^{\lambda=1} - E_P. \tag{13}$$

After a simulation reaches equilibrium, the total, kinetic, and potential energies are blocked and uncertainties estimated. In our calculations we have set $\delta = 10^{-4}$.

The walker displacements and the estimates of E_{ℓ}^{λ} conform with the standard DMC method. The second step for a new generation of walkers, the branching (birth-death process), is needed to avoid keeping walkers with very little weights, which

at the end of the calculation do not contribute to the results. With minimal generalizations, this step also follows common rules in the literature [30].

(i) A walker is copied if all of its weights are greater than 2. Each copy bears half of the original weights.

(ii) Walkers with at least one weight between a threshold of w_{thr} and 2 are kept without changes.

(iii) Walkers with all of their weights less than w_{thr} are candidates to be combined according to the following rules. For a given walker i and each value of λ, the weight ω_i^λ is treated independently of the other walker weights. If walkers i and j satisfy the condition of being combined, then with probability $\frac{w_i^\lambda}{w_i^\lambda+w_j^\lambda}$ the weight $w_i^\lambda + w_j^\lambda$ is attributed to walker i and the value zero is attributed to walker j. The sum of weights is attributed to walker j with probability $1 - \frac{w_i^\lambda}{w_i^\lambda+w_j^\lambda}$ and the value zero is attributed to walker i. If for a particular λ the sum of the two weights is equal to zero, both walkers keep this value.

(iv) Delete a walker if all its weights are equal to zero.

The value of w_{thr} is chosen by analyzing a compromise between two conflicting requirements. Ideally, w_{thr} needs to be small to avoid walkers with one or two of their weights equal to zero. These walkers are undesirable, because they spoil the correlation we need to achieve accurate numerical derivatives. On the other hand, we do not want to carry walkers with weights that are too low during the simulation. In our simulations we have verified that $w_{\text{thr}} = 0.3$ offers a good compromise between these two requirements.

One procedure we employ to avoid fluctuations of the walker population is the dynamic adjustment of trial energies. In our calculations the update was made every 20 generations using the following expression:

$$E_{\text{trial}}^\lambda = E_b^\lambda + \frac{C_0}{\tau_2 - \tau_1} \ln\left(\frac{W^\lambda(\tau_2)}{W_0}\right), \tag{14}$$

where E_b^λ is the total energy averaged over a block of the last 20 generations, C_0 is a parameter which smooths the fluctuations in the sum of the weights, $\tau_2 - \tau_1$ is the time interval since the last update, W^λ is the sum of the ω_i^λ weights of all walkers at time τ_2, and W_0 is a constant, the target value for the sum of weights. The value of W_0 is approximately equal to the number of walkers kept during the simulation. The time τ_i is related to the performed number of generations M_i through $\tau_i = M_i \Delta\tau$, where $\Delta\tau$ is the time step used in Eq. (9). The update of the trial energies according to Eq. (14) together with the chosen value for w_{thr} has allowed runs where all the walkers did not have any weight equal to zero. The expression of Eq. (15) is reminiscent of energy calculation by the growth estimator

$$E_g^\lambda = E_{\text{trial}}^\lambda + \frac{1}{\tau_2 - \tau_1} \ln\left(\frac{W^\lambda(\tau_1)}{W^\lambda(\tau_2)}\right). \tag{15}$$

C. Simulations

In our investigation of the properties of bulk helium we impose periodic boundary conditions. The cutoff convention, the distance beyond which correlation among the atoms is set to zero, is enforced at half of the smallest box size. Distances between pairs of particles are computed by the minimum-image convention. Tail correction, a correction to the total potential energy, is made by integrating the two-body interatomic potential from the cutoff distance up to infinity. We assume a radial pair distribution function equal to 1 beyond the cutoff distance. We performed simulations in the solid phase, using cells with 180 and 288 particles. In the liquid phase, 180 atoms were considered. In both phases the simulations start from crystalline structures. Enough initial configurations were discarded to assure converged samples of $\psi_G(\mathbf{R})\psi_0(\mathbf{R})$. The acceptance ratio was made greater than 99%, so that our statistical errors are greater than those due to the adopted time step, $\Delta\tau = 0.001\ \text{K}^{-1}$ [19,30].

D. Bias analyses

The effort to increase the level of accuracy of DMC results is an active field of research [26,31]. In our work we applied several approaches to minimize the fluctuations in the walker population. As already mentioned, walkers with small statistical weights are combined (see Sec. II B). This is an improvement of the common truncation method, where the weights are always kept equal to 1. This is accomplished by taking the integer part of the computed weight plus a random number from the standard uniform distribution and, eventually, making copies of the walkers. We also employ a dynamic adjustment for the trial energy, Eq. (14), and an effective time step, Eq. (11). These procedures assist in reducing bias in our calculations and consequently increase the level of accuracy of the DMC results. It is also important to avoid fluctuations in the walker population to take full advantage of the distributed parallel machines. In this case, the issue is the load balance that may become a bottleneck to acquiring high accuracy as allowed by the continuous increase of the number of computing nodes [31]. However, it will be useful to verify how our algorithm is performing under variations of the number of walkers in the target population and also how the results depend on the number of atoms used to simulate bulk ^{4}He.

1. Number of walkers

From their inception, it has been known that projector methods are subjected to bias due to the walker population control applied. As these methods became more widely spread, many procedures were put forward to minimize fluctuations of the population. The dynamic adjustment of the trial energy we use, Eq. (14), is one of the most efficient methods for population control [31]. Although one might consider this procedure as a source of bias, in reality, if it is implemented in a judicious way, an automatic adjustment of the trial energy can result in small changes to this quantity and thus lessen its consequences.

It is also true that, as the target population increases, the relative change in the number of walkers due to an update of the trial energy decreases, and as a consequence the resulting bias also decreases. In this context it is useful to verify how quantities of interest may vary with the target number of walkers in the simulations. We have conducted this study and our results are presented in Table I. Although most of our simulations were performed with a number of walkers $N_W = \mathcal{O}(10^3)$, we see that even with a modest number ($N_W = 400$)

TABLE I. Total ε_T, kinetic ε_K, and potential ε_P energies per particle in units of kelvin for the given average number of walkers, N_W. The simulations in the solid phase were made in an hcp structure with 180 atoms and at the density $\rho\sigma^3 = 0.549, \sigma = 2.556$ Å. Results were obtained with the NJ guiding function.

N_W	ε_T (K)	ε_K (K)	ε_P (K)
400	-4.49 ± 0.01	30.79 ± 0.08	-35.28 ± 0.08
1000	-4.49 ± 0.01	30.82 ± 0.07	-35.31 ± 0.07
2000	-4.49 ± 0.01	30.75 ± 0.08	-35.24 ± 0.08
3000	-4.49 ± 0.01	30.78 ± 0.06	-35.27 ± 0.06

any possible bias lies inside the statistical uncertainties of the total, kinetic, and potential energies.

Findings of Cerf and Martin [25] corroborate our conclusions that a number of walker of the order of 10^3 is enough to assure that a possible bias in the calculations are within the statistical uncertainties. Although according to Ref. [25] a finite size of the population of random walkers and its consequences can be taken into account by using an effective mass $m^* = (1 - \frac{1}{N_W})$, in our case, it would not produce practical results because this correction would lead to results that lie already within our statistical uncertainties.

2. *Number of atoms*

We have also conducted studies about finite size effects in the results. Simulations were made at the density $\rho\sigma^3 = 0.549$ of the solid phase starting from an hcp structure. In Fig. 1, we display the results of Table II for the total energy as a function of the number of atoms in the simulations. In the same figure, we show for the corresponding number of atoms the tail correction. The values of the kinetic and potential energies of these simulations, also presented in Table II, are plotted in Fig 2. As we can verify, only at the lowest number of atoms considered ($N = 144$) can some bias be present

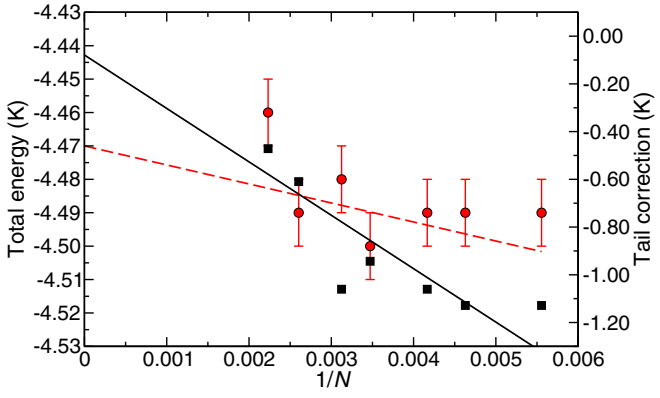

FIG. 1. Linear fit to the total energy per atom as a function of the inverse of the number of particles at the density $\rho\sigma^3 = 0.549$ (left hand scale, red circles and dashed line). Exact values are shown for the tail correction of the two-body potential for the corresponding number of atoms (right hand scale, black squares). The black line is a linear fit to these values. Deviations from a smooth behavior of this quantity are due to a discontinuous change in the smallest size of a simulation cell built to accommodate an hcp crystalline structure.

TABLE II. Results for the total ε_T, kinetic ε_K, and potential ε_P energies per particle in units of kelvin for the given numbers N of atoms considered in the simulations. All the results were obtained starting from an hcp structure at the density $\rho\sigma^3 = 0.549$. The NJ guiding function and approximately 2000 random walkers were used. The last line shows results for the bulk system obtained from linear extrapolation of the system.

N	ε_T (K)	ε_K (K)	ε_P (K)
144	-4.59 ± 0.01	30.99 ± 0.08	-35.58 ± 0.08
180	-4.49 ± 0.01	30.76 ± 0.09	-35.25 ± 0.09
216	-4.49 ± 0.01	30.81 ± 0.08	-35.30 ± 0.08
240	-4.49 ± 0.01	30.83 ± 0.08	-35.32 ± 0.08
288	-4.50 ± 0.01	30.82 ± 0.09	-35.32 ± 0.09
320	-4.48 ± 0.01	30.74 ± 0.09	-35.22 ± 0.09
384	-4.49 ± 0.01	30.84 ± 0.07	-35.33 ± 0.07
448	-4.46 ± 0.01	30.85 ± 0.06	-35.31 ± 0.06
∞	-4.465 ± 0.013	30.87 ± 0.10	-35.34 ± 0.10

in the results, a fact that can probably be attributed to the approximation of the radial pair distribution function, which is assumed to be 1, in the calculation of the tail correction. Simulations with 180 or more atoms show that the results for the total, kinetic, and potential energies are in excellent agreement among themselves. For this reason, only values obtained with 180 or more atoms were considered in the linear fits. They were obtained by the standard weighted least squares method. In the fits, we considered as weights the reciprocal values of the variance of the computed quantities. From the extrapolation, $1/N \to 0$, it is safe to say that size effects are within the statistical uncertainties of our results.

III. RESULTS

The characterization of the liquid-solid phase transition requires the equation of state (EOS) for both phases. For the solid phase, we have computed the EOS using SNJ and NJ guiding functions. The EOS for ^{4}He, in the liquid phase, was computed in some detail using a simple Jastrow

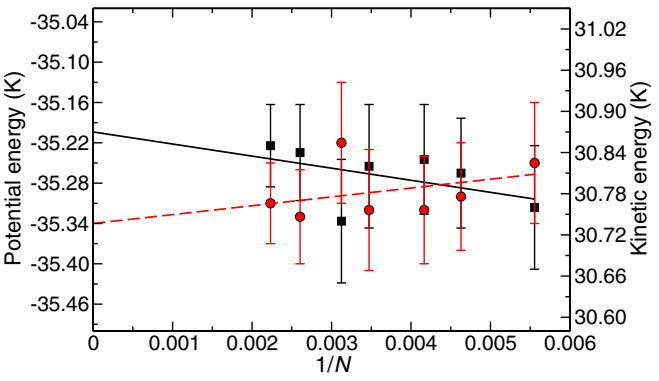

FIG. 2. Kinetic (right hand scale, black squares) and potential energy (left hand scale, red circles) per atom as a function of the inverse of the number of particles at the density $\rho\sigma^3 = 0.549$. The solid line is a linear fit to the kinetic energy results and the dashed line is a linear fit to those of the potential energy.

TABLE III. Total ε_T, kinetic ε_K, and potential ε_P energies per particle in units of kelvin for the solid phase at the given densities. Results were obtained with NJ and SNJ guiding functions.

$\rho\sigma^3$	ε_T (K)		ε_K (K)		ε_P (K)
	NJ	SNJ	NJ	SNJ	NJ
0.5026	-5.73 ± 0.01	-5.70 ± 0.01	26.40 ± 0.07	26.61 ± 0.05	-32.13 ± 0.07
0.5126	-5.53 ± 0.01	-5.53 ± 0.02	27.32 ± 0.06	27.40 ± 0.10	-32.85 ± 0.06
0.5277	-5.17 ± 0.01	-5.20 ± 0.01	28.67 ± 0.07	28.73 ± 0.05	-33.84 ± 0.07
0.5344	-4.96 ± 0.01	-4.93 ± 0.01	29.33 ± 0.07	29.85 ± 0.05	-34.29 ± 0.07
0.5494	-4.50 ± 0.01	-4.50 ± 0.02	30.82 ± 0.09	30.99 ± 0.07	-35.32 ± 0.09
0.5694	-3.79 ± 0.01	-3.70 ± 0.01	32.90 ± 0.07	33.15 ± 0.05	-36.69 ± 0.07
0.5895	-2.83 ± 0.01	-2.80 ± 0.01	34.79 ± 0.08	35.10 ± 0.10	-37.62 ± 0.08

guiding function. The kinetic and potential energies were also estimated.

A. Solid phase

The total energy per ^{4}He atom in the solid phase was estimated starting from a defect free crystalline structure hcp. Our results are presented in Table III. Equations of state were determined by fits of our results to functions of the form

$$\varepsilon(\rho) = \varepsilon_0 + B\left(\frac{\rho-\rho_0}{\rho_0}\right)^2 + C\left(\frac{\rho-\rho_0}{\rho_0}\right)^3, \qquad (16)$$

where ε_0, B, C, and ρ_0 are fitting parameters. The fitted values are displayed in Table IV and the resulting EOSs for SNJ and NJ guiding functions are shown in Fig. 3. The binding energies determined from the EOS for both of the guiding functions are in general in good agreement with the DMC results.

The DMC energies have slightly lower values than those from experiment. This situation can be attributed to a lack of three-body interactions in the interatomic potential [35,36]. This effect becomes more pronounced as the density increases in agreement with Ref. [37]. The total energies at the level of precision we have considered, obtained with the NJ guiding function, are indistinguishable within statistical uncertainty or are marginally lower than those determined with SNJ. The only exception is at $\rho\sigma^3 = 0.5694$ where the computed energies are not in agreement. This result can be explained arguing the following. Although a NJ guiding function disregards a fundamental property of the system, viz., symmetry under particle interchange, it still has an important superposition with the system ground state. Most likely, the NJ guiding function misses configurations of low probability, that contribute with very small weights in the calculation of the energy. In other words, for the system under consideration, the atoms in the crystalline phase could be treated as distinguishable particles, a conclusion also supported by path integral calculations [38].

The kinetic energies per particle as a function of the density, estimated through the Feynman-Hellmann theorem, presented in Table III, are plotted in Fig. 4. Even though the linear behavior of this quantity with the density is experimentally observed above the λ transition [41], we decided to fit our zero temperature results using the same functional dependence. In the solid phase the kinetic energies obtained with the SNJ guiding function are higher than those determined using NJ, except at the three lowest densities where they are indistinguishable, within statistical uncertainties. This trend is not obvious, since atoms are in principle less localized with the SNJ guiding function.

TABLE IV. Fitting parameters for the EOS in the solid and liquid phases for the given importance function.

Importance function	ε_0 (K)	B (K)	C (K)	$\rho_0\sigma^3$
		Solid phase		
SNJ	-5.91 ± 0.06	72 ± 20	-70 ± 27	0.476 ± 0.005
NJ	-6.1 ± 0.2	51 ± 27	-40 ± 61	0.46 ± 0.02
		Liquid phase		
J	-7.260 ± 0.002	15.3 ± 0.2	-14 ± 2	0.352 ± 0.001

B. Liquid phase

Estimates of the total energy per ^{4}He atom as a function of the density are shown in Fig. 5. The liquid EOS was determined by a fit of our results to Eq. (16). The values of the fitted parameters are presented in Table IV. In the liquid phase, the fitted parameter ρ_0 stands for the equilibrium density of the system. Our fitted value is lower than the

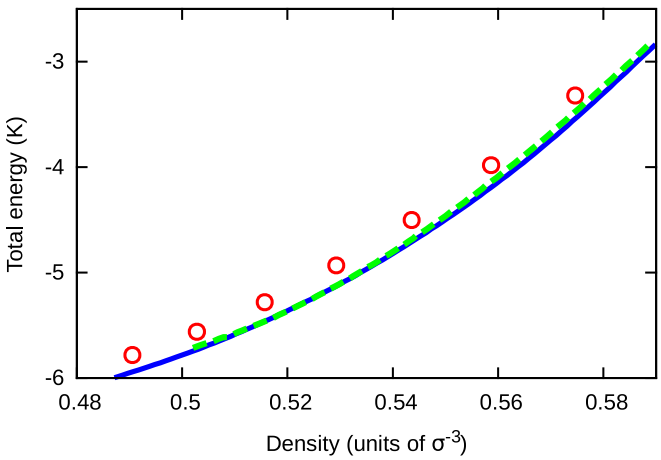

FIG. 3. Total energy per atom as a function of the density in the solid phase. The curves stand for fits to the estimated values of the energies using Eq. (16); the dashed green line stands for those obtained with the SNJ guide function; those for NJ are shown by a blue line. The curves are hard to distinguish at the figure resolution. Experimental data [32–34] are displayed by red circles.

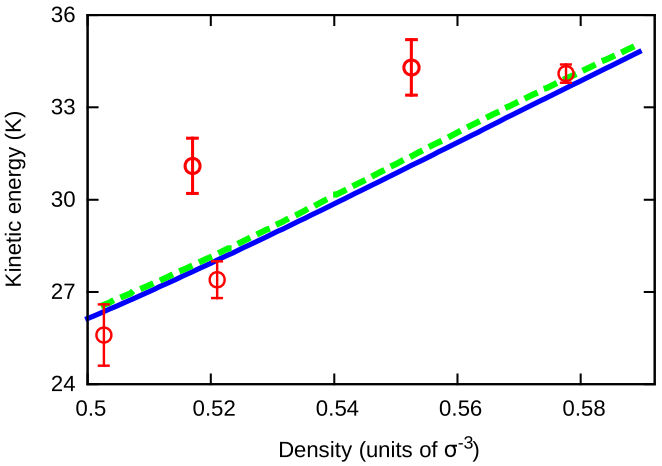

FIG. 4. Kinetic energy per atom as a function of the density in the solid phase. The curves stand for fits to the estimated values. Results for the SNJ guide function are displayed by a dashed green line; those for NJ are shown with a blue solid line. Experimental data [33,34,39,40] are displayed by red circles.

experimental value, $\rho_0\sigma^3 = 0.3649$ [45]. Also in this phase, the discrepancies between theory and experiment can be attributed to a lack of a three-body interatomic interaction in our model Hamiltonian [46]. In general, the total energies are also in good agreement with experimental data obtained at small but finite temperatures.

For completeness, we also present in Fig. 6 estimated values of the kinetic energy fitted to a parabola, even if the quadratic behavior was inferred from experimental data obtained at a temperature above the λ transition [41].

The kinetic energy values in the liquid phase are lower than those found for the solid phase. This is mainly a consequence of the zero-point motion effect due to Heisenberg's uncertainty principle [47,48]. Although the zero-point kinetic energy is the main reason why systems of helium atoms solidify only

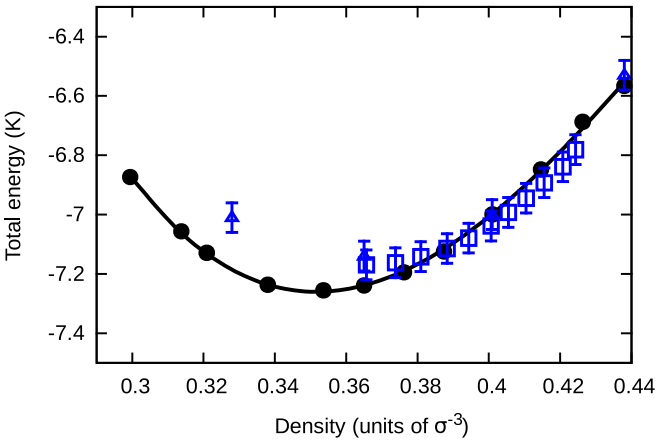

FIG. 5. Equation of state as a function of the density in the liquid phase. The curve stands for a fit to the estimated values of the energies using Eq. (16). Our numerical results are displayed by solid black circles. Errors are smaller than the symbol size. Experimental data for the liquid phase [42,43] are shown by squares. The triangles stand for values determined at $T = 0.05$ K [44].

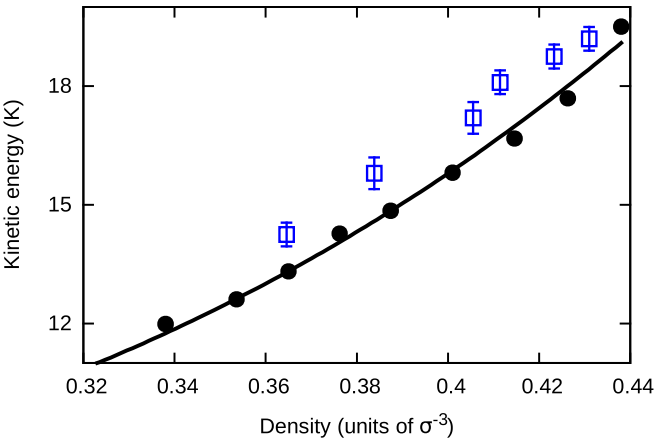

FIG. 6. Kinetic energy per atom as a function of the density in the liquid phase. The curve stands for a fit to the estimated values displayed by solid black circles. Errors are smaller than the symbol size. The squares represent experimental results [44].

under the external pressure of about 25 atm, other quantum mechanical phenomena might also be of importance [22].

C. Solid-liquid phase transition

Systems formed from ^{4}He atoms at absolute zero temperature present a liquid-solid phase transition under variations of pressure, a nonthermal parameter. We have calculated the freezing (ρ_f) and melting (ρ_m) densities assuming a first-order transition by two methods and for the two guiding functions we are considering. The first is the well known double-tangent Maxwell construction. A line tangent to both liquid and solid equations of state in a diagram of the Helmholtz free energy F as a function of volume V is built. This condition arises since it is expected that in the transition the system will behave as a linear combination of both phases. The tangent line to both the liquid and solid EOS is the path that minimizes the Helmholtz free energy, i.e., the equilibrium situation. The two points with the same pressure will delimit the density interval in which the phase transition occurs. So, the conditions for determining the freezing and melting densities can be written as

$$-\left(\frac{\partial F}{\partial V_1}\right)_T = -\left(\frac{\partial F}{\partial V_2}\right)_T \text{ (equal pressure)} \qquad (17)$$

and

$$\frac{\partial F}{\partial V_1} = \frac{F_2 - F_1}{V_2 - V_1} \text{ (common tangent).} \qquad (18)$$

For the case $T = 0$ K, we can rewrite it as

$$\rho_1^2 \frac{\partial \varepsilon}{\partial \rho_1} = \rho_2^2 \frac{\partial \varepsilon}{\partial \rho_2}, \qquad (19)$$

$$-\rho_1^2 \frac{\partial \varepsilon}{\partial \rho_1} = \frac{\varepsilon_2 - \varepsilon_1}{1/\rho_2 - 1/\rho_1}. \qquad (20)$$

Our results are given in Table V.

In the second method, the quantities ρ_f and ρ_m were obtained by performing a thermodynamic analysis of the EOS as done in Ref. [12]. The first-order transition is characterized by a discontinuity at the transition pressure of the Gibbs free

TABLE V. Freezing and melting densities for the given calculation method and guiding function, in the solid phase. In the liquid phase, the guiding function is of the Jastrow form. The experimental datum is from Ref. [49].

Guide function	$\rho_f\sigma^3$	$\rho_m\sigma^3$
	Double tangent construction	
NJ	0.417 ± 0.027	0.483 ± 0.051
SNJ	0.424 ± 0.030	0.489 ± 0.095
	Thermodynamic analysis	
NJ	0.422 ± 0.044	0.486 ± 0.050
SNJ	0.424 ± 0.096	0.489 ± 0.097
	Experimental	
	0.438	0.484

energy G as a function of the pressure. For the calculation of the Gibbs free energy, we first compute the pressure through the fitted lines of the EOS for both phases:

$$p(\rho) = \rho^2 \frac{\partial \varepsilon(\rho)}{\partial \rho}. \tag{21}$$

The Gibbs free energy per particle g is then easily calculated using the relation

$$g = \frac{G}{N} = \varepsilon + \frac{p}{\rho}. \tag{22}$$

Our result for the Gibbs free energy per particle as a function of the pressure is exhibited in Fig. 7. The pressure at the phase transition is estimated by determining the intersection of the fitted curves for the liquid and solid phases of the Gibbs free energy, where small kinks appear. On them, the Gibbs free energy per particle is equal to the chemical potential. And at the transition, the chemical potential has a single value in the liquid and solid phases. The calculation made with the SNJ

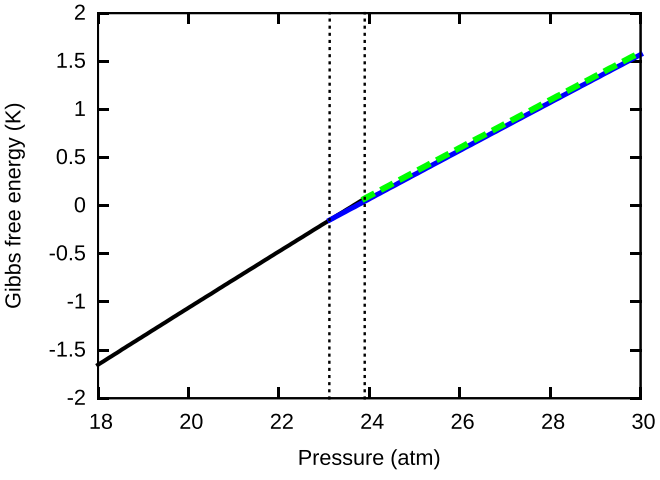

FIG. 7. The Gibbs free energies per particle as a function of pressure. Results in the liquid phase are shown by a black line. In the solid phase the dashed green line stands for values obtained with the SNJ guide function and the blue one stands for those determined with NJ. The left vertical dotted line identifies the transition pressure (the discontinuity) obtained with the NJ guiding function and the right one identifies that with SNJ.

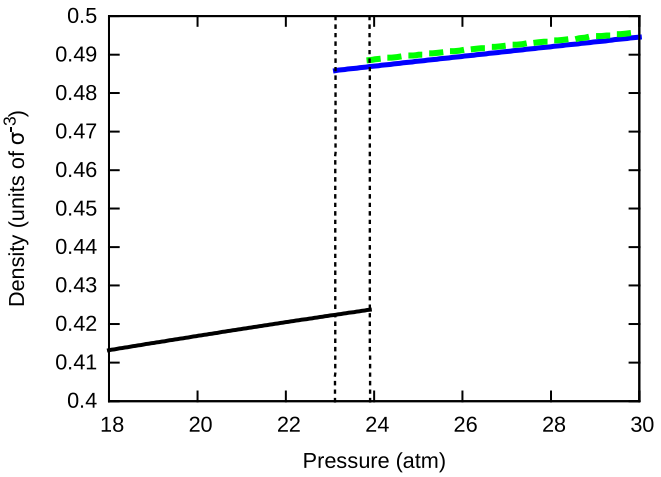

FIG. 8. Density as a function of the pressure. The solid black line stands for results in the liquid phase. In the solid phase the green dashed line and the blue line show results for SNJ and NJ guiding functions, respectively. The dotted vertical lines indicate the transition pressures; the left one is for the NJ guiding function and the right one is for SNJ.

guiding function gives an estimate of the transition pressure as 24 ± 5 atm. The one performed with NJ gives a value of 23 ± 3 atm. Both estimates are in good agreement with the experimental datum of about 25 atm for this transition [49].

The pressure of the solid-liquid transition can be used to determine the melting and freezing densities. In Fig. 8, we display the density as a function of the pressure. In Table V, we show the values of ρ_f and ρ_m obtained in this way.

The values of the freezing and melting densities calculated with the two guiding functions, using either the Maxwell construction or the thermodynamic analysis, agree between themselves. Moreover, both values are in excellent agreement with the experimental values.

IV. FINAL COMMENTS

Results obtained for the solid phase of ^{4}He atoms employing the NJ and SNJ guiding functions in the diffusion Monte Carlo method are practically equivalent. To some extent, this outcome is surprising because SNJ restores a fundamental property of the system, the symmetry under particle exchange. A possible explanation for this might be found in the nature of this quantum solid. If on the one hand the harmonic approximation completely breaks down, due to long excursions of the atoms from the lattice sites, on the other hand, exchange is rare in quantum solids [38,50] and can be neglected. This argument also clarifies why DMC calculations that use a guiding function which disregards symmetry under particle exchange are in agreement with the experiment [35].

The trend observed for kinetic energy as a function of density in the solid phase and the values of pressure in the solid-liquid phase transition might induce a conclusion that results obtained with the SNJ guiding function are slightly better than those using the NJ. However, the statistical uncertainties prevent a conclusive statement. Nevertheless, the estimated values of both these quantities are in good agreement with the experiment. The EOSs in the solid phase obtained through the

two guiding functions are also of the same quality, probably because the exchange energy is very small.

Because the SNJ restores symmetry under particle exchange, the price to be paid in a simulation for its slightly more evolved form is justified. An issue that might also be of interest in this context is the ergodicity of the sampling. It would be interesting to know how the algorithm that uses the SNJ guiding function compares to one that considers the symmetrization through a permanent.

In summary, the explicit introduction of the Nosanow one-body term that localizes ^{4}He atoms around lattice sites is able to produce reasonable results. In a much more recent effort, the symmetry under particle exchange without the need of a permanent was implemented [6]. The translational invariance is a fundamental aspect that has not yet been contemplated in developments seeking explicit functional forms in the description of solid helium. When this requirement is accomplished, many opportunities will open for the investigation of quantum solids at zero temperature, for instance, the study of phase transitions of ^{4}He films in substrates. We hope that this paper will prompt efforts to devise an explicit translational invariant wave function where a solid phase emerges as a consequence of a symmetry breaking due only to many-body effects. We believe that further endeavors in this direction will bring great benefit to the understanding of quantum solids and in particular for those formed from helium atoms.

ACKNOWLEDGMENTS

The authors acknowledge financial support from the Brazilian agencies Fundação de Amparo à Pesquisa do Estado de São Paulo (FAPESP), Fundação de Amparo à Pesquisa do Estado de Rio de Janeiro (FAPERJ), and Conselho Nacional de Desenvolvimento Científico e Tecnológico (CNPq). Part of the computations were performed at the Centro Nacional de Processamento de Alto Desempenho em São Paulo (CENAPAD-SP), a high-performance computing facility at Universidade Estadual de Campinas.

[1] S. Balibar, J. Beamish, and R. Hallock, J. Low Temp. Phys. **180**, 3 (2015).
[2] Z. G. Cheng, J. Beamish, A. D. Fefferman, F. Souris, S. Balibar, and V. Dauvois, Phys. Rev. Lett. **114**, 165301 (2015).
[3] Y. Vekhov, W. J. Mullin, and R. B. Hallock, Phys. Rev. Lett. **113**, 035302 (2014).
[4] A. Haziot, X. Rojas, A. D. Fefferman, J. R. Beamish, and S. Balibar, Phys. Rev. Lett. **110**, 035301 (2013).
[5] E. Feenberg, J. Low Temp. Phys. **16**, 125 (1974).
[6] C. Cazorla, G. E. Astrakharchik, J. Casulleras, and J. Boronat, New J. Phys. **11**, 013047 (2009).
[7] S. A. Vitiello and K. E. Schmidt, Phys. Rev. B **46**, 5442 (1992).
[8] S. Vitiello, K. Runge, and M. H. Kalos, Phys. Rev. Lett. **60**, 1970 (1988).
[9] K. Schmidt, M. H. Kalos, M. A. Lee, and G. V. Chester, Phys. Rev. Lett. **45**, 573 (1980).
[10] S. A. Vitiello and K. E. Schmidt, Phys. Rev. B **60**, 12342 (1999).
[11] T. MacFarland, S. A. Vitiello, L. Reatto, G. V. Chester, and M. H. Kalos, Phys. Rev. B **50**, 13577 (1994).
[12] Y. Lutsyshyn, G. E. Astrakharchik, C. Cazorla, and J. Boronat, Phys. Rev. B **90**, 214512 (2014).
[13] Y. Lutsyshyn, Phys. Rev. B **92**, 214507 (2015).
[14] Y. Lutsyshyn, J. Chem. Phys. **146**, 124102 (2017).
[15] V. R. Pandharipande and H. A. Bethe, Phys. Rev. C **7**, 1312 (1973).
[16] C. J. Umrigar, J. Toulouse, C. Filippi, S. Sorella, and R. G. Hennig, Phys. Rev. Lett. **98**, 110201 (2007).
[17] R. J. Needs, M. D. Towler, N. D. Drummond, and P. L. Rios, J. Phys.: Condens. Matter **22**, 023201 (2010).
[18] W. M. C. Foulkes, L. Mitas, R. J. Needs, and G. Rajagopal, Rev. Mod. Phys. **73**, 33 (2001).
[19] P. J. Reynolds, D. M. Ceperley, B. J. Alder, and W. A. Lester, J. Chem. Phys. **77**, 5593 (1982).
[20] R. Feynman, Int. J. Theor. Phys. **21**, 467 (1982).
[21] L. Brualla, S. Fantoni, A. Sarsa, K. E. Schmidt, and S. A. Vitiello, Phys. Rev. C **67**, 065806 (2003).
[22] M. Boninsegni, L. Pollet, N. Prokof'ev, and B. Svistunov, Phys. Rev. Lett. **109**, 025302 (2012).
[23] S. Ujevic and S. A. Vitiello, J. Chem. Phys. **119**, 8482 (2003).
[24] H. Glyde, J. Low Temp. Phys. **172**, 364 (2013).
[25] N. Cerf and O. C. Martin, Phys. Rev. E **51**, 3679 (1995).
[26] J. D. Mallory, S. E. Brown, and V. A. Mandelshtam, J. Phys. Chem. A **119**, 6504 (2015).
[27] S. A. Vitiello, J. Chem. Phys. **134**, 054102 (2011).
[28] R. A. Aziz, A. R. Janzen, and M. R. Moldover, Phys. Rev. Lett. **74**, 1586 (1995).
[29] P. A. Whitlock, D. M. Ceperley, G. V. Chester, and M. H. Kalos, Phys. Rev. B **19**, 5598 (1979).
[30] C. J. Umrigar, M. P. Nightingale, and K. J. Runge, J. Chem. Phys. **99**, 2865 (1993).
[31] J. T. Krogel and D. M. Ceperley, in *Advances in Quantum Monte Carlo*, edited by S. Tanaka, S. M. Rothstein, and W. A. Lester, Jr. (American Chemical Society, Washington, DC, 2012), Chap. 2, pp. 13–26.
[32] D. O. Edwards and R. C. Pandorf, Phys. Rev. **140**, A816 (1965).
[33] M. A. Adams, J. Mayers, O. Kirichek, and R. B. E. Down, Phys. Rev. Lett. **98**, 085301 (2007).
[34] R. C. Blasdell, D. M. Ceperley, and R. O. Simmons, Z. Naturforsh. **48a**, 433 (1993).
[35] S. Ujevic and S. A. Vitiello, J. Phys.: Condens. Matter **19**, 116212 (2007).
[36] S. Ujevic and S. A. Vitiello, Int. J. Mod. Phys. B **20**, 5103 (2006).
[37] A. L. Barnes and R. J. Hinde, J. Chem. Phys. **146**, 094510 (2017).
[38] D. M. Ceperley, Rev. Mod. Phys. **67**, 279 (1995).
[39] S. O. Diallo, J. V. Pearce, R. T. Azuah, and H. R. Glyde, Phys. Rev. Lett. **93**, 075301 (2004).
[40] R. O. Hilleke, P. Chaddah, R. O. Simmons, D. L. Price, and S. K. Sinha, Phys. Rev. Lett. **52**, 847 (1984).
[41] U. Bafile, M. Zoppi, F. Barocchi, R. Magli, and J. Mayers, Phys. Rev. Lett. **75**, 1957 (1995).
[42] R. D. B. Ouboter and C. N. Yang, Physica B+C **144**, 127 (1987).

[43] R. A. Aziz and R. K. Pathria, Phys. Rev. A **7**, 809 (1973).
[44] H. R. Glyde, S. O. Diallo, R. T. Azuah, O. Kirichek, and J. W. Taylor, Phys. Rev. B **84**, 184506 (2011).
[45] P. R. Roach, J. B. Ketterson, and C.-W. Woo, Phys. Rev. A **2**, 543 (1970).
[46] S. Ujevic and S. A. Vitiello, Phys. Rev. B **73**, 012511 (2006).
[47] J. E. Hirsch, Mod. Phys. Lett. B **25**, 2219 (2011).
[48] D. M. Ceperley, R. O. Simmons, and R. C. Blasdell, Phys. Rev. Lett. **77**, 115 (1996).
[49] E. R. Grilly, J. Low Temp. Phys. **11**, 33 (1973).
[50] D. M. Ceperley and B. Bernu, Phys. Rev. Lett. **93**, 155303 (2004).